Fusion Engineering and Design 192 (2023) 113775

Contents lists available at ScienceDirect

Fusion Engineering and Design

journal homepage: www.elsevier.com/locate/fusengdes

White noise characterization and thermo-mechanical analysis of DTT pick-up coils

M. Lacquaniti [a,*], G. Sias [a], A. Fanni [a], A. Pironti [b,c], F. Giorgetti [d,e], G. Calabrò [d], E. Aymerich [a], M. Baruzzo [e]

[a] Department of Electrical and Electronic Engineering, University of Cagliari, via Marengo 2, Cagliari 09123, Italy
[b] Department of Electrical Engineering and Information Technology, University of Napoli Federico II, via Claudio 21, Napoli 80125, Italy
[c] CREATE Consorzium, via Claudio 21, Napoli 80125, Italy
[d] Department of Economy, Engineering, Society and Business (DEIm), University of Tuscia, Largo dell'Università snc, Loc. Riello, Viterbo 01100, Italy
[e] ENEA, Department of Fusion and Nuclear Safety Technology, for EUROfusion, Via E. Fermi 45, 00044 Frascati (Roma), Rome, Frascati 00044, Italy

ARTICLE INFO

Keywords:
DTT
Ex -vessel pick-up coil
In-vessel pick-up coil
Probe white noise characterization
Inverse boundary reconstruction
Bulk analysis
Thermomechanical analysis

ABSTRACT

The Divertor Tokamak Test (DTT) [1] is presently in the start-up phase of construction. Among diagnostics, the magnetic ones are the first components that will have to be ready for installation and commissioning when DTT vacuum vessel and magnets will be assembled. In this paper, the white noise characterization of DTT in-vessel pick up coil measurements and the thermo-mechanical analysis of ex-vessel pick up coils will be presented referring to the 2021 probe configuration. In particular, the systematic error due to white noise affecting the 80 internal pick-up coil measurements on plasma position reconstruction has been assessed. Such plasma reconstruction has been done by assuming a filamentary representation of the plasma current density. The effect of noise on the measurements is characterized evaluating the mean error, the mean square error and the standard deviation, on the difference between the noisy inverse reconstruction and the ideal inverse reconstruction evaluated on suitable plasma-wall gaps.

Moreover, a feasibility study of mounting a torlon pick-up coil between the vacuum vessel and the thermal shield, in terms of bulk has been developed. In addition, the probe thermomechanical stresses are preliminarily investigated for backing and operative conditions, assuming a welding as mounting solution. The study shows that no bulk criticality is present for mounting the external pick-up coil. The operative temperature results to be far from thermomechanical critical condition. On the contrary, the baking temperature $T = 220\ ^\circ C$ presents some critical issues. The achieved results are propaedeutic to make more detailed choice in the following design steps, such as the probe fixing solution, the bolt dimension and the materials. When detailed pick-up coils mounting solution will be defined, the stresses on the contact region between the pick-up coils and the vacuum vessel accurately evaluate.

1. Introduction

In a tokamak device, magnetic diagnostics plays a key role in the understanding of plasma physics, machine protection, plasma control, and equilibrium reconstruction. The magnetic diagnostics system includes measurements of magnetic fluxes, plasma current, and diamagnetic flux made inside and outside the vacuum vessel [2–3]. In-vessel and ex-vessel pick-up coils are electromagnetic transducers addressed to the local magnetic field measurements.

Characterization of white noise, affecting the pick-up coil measurements, is a key design driving requirement for the plasma equilibrium reconstruction. To this purpose, Section 2 is devoted to the characterization of the systematic error on the inverse boundary reconstruction due to white noise referring to 2021 DTT probe configuration [4]. In particular, Section 2.1 reports the magnetic reference configuration and the input parameters for the inverse reconstruction. Section 2.2 reports the optimization of the pseudo-inverse reconstruction tolerance in presence of noisy measurements. Finally, in Section 2.3 the effect of noise on the measurements is presented in terms of the mean error (ME), the mean square error (MSE), and variance (σ^2) on the gap

* Corresponding author.
E-mail address: massimiliano.lacquaniti@unica.it (M. Lacquaniti).

https://doi.org/10.1016/j.fusengdes.2023.113775
Received 11 October 2022; Received in revised form 6 April 2023; Accepted 20 April 2023
Available online 5 May 2023

evaluation, and in terms of maximum and mean error in percentages on the plasma current value and the plasma barycenter position.

Concerning the feasibility study of mounting an ex-vessel probe [4], Section 3 reports a FEM analysis aimed to evaluate the mounting bulk and thermomechanical stresses. The bulk available for the probe mounting is verified by evaluating the vacuum vessel (VV) thermal expansion. In addition, a thermomechanical analysis has been developed to preliminarily investigate the mechanical stresses on the pick-up coil and the screw due to both the different thermal expansion of materials and the VV dilatation, for both operative and baking conditions. The developed study allows us to estimate the external probe rotation and VV displacement during the operative conditions, which are essential in view of evaluating the inverse boundary reconstruction error by the external probe measurements. In Section 3.1 the main thermal and structural assumptions are reported. The results of the steady-state thermal analyses are reported in Section 3.2, whereas static structural analysis is presented in Section 3.3.

2. Systematic error characterization for the inverse boundary reconstruction

In this section, a procedure to evaluate the systematic error on the inverse boundary reconstruction due to a white noise has been developed. The white noise characterization is needed to guarantee high performance in several fields, such as the plasma magnetic control, which must rely on an accurate shape reconstruction. Thus, the reliability of the measurements totally affects the equilibrium reconstruction.

The algorithm for the inverse boundary reconstruction determines the plasma boundary from the poloidal field coil currents and by assuming a filamentary representation of the plasma current density [5]. The poloidal flux map is computed by the Eq. (1):

$$\psi(\boldsymbol{r}) = \int_{R^2} G_0(\boldsymbol{r},\widetilde{\boldsymbol{r}}) J_\varphi(\widetilde{\boldsymbol{r}}) d\widetilde{S} \tag{1}$$

where $G_0$is the Free Space Green's Function, which represents the flux produced by an infinitesimal toroidal filament carrying a unitary current and J_φ is the toroidal current. As shown in [5], the use of G_0 allows the discretization of the problem. Thus, the inverse boundary reconstruction problem can be faced as a FEM problem described by Eq. (2):

$$|\psi|^{n\times 1} = |G_{0\psi}|^{n\times(n_{coil}+n_{el})} \cdot |i|^{(n_{coil}+n_{el})\times 1} \tag{2}$$

where, n is the number of the mesh nodes in the whole domain, n_{coil} is the number of the active current filaments (i_{coil}), located at the mesh element barycentre inside the poloidal field coil domains, and n_{el} is the number of fictitious currents i_{el} placed on ellipse located inside the possible plasma region (magenta line in Fig. 1). Among the currents i, those from the active coils are provided as inputs, whereas the values and the number of the fictitious plasma current filaments need to be optimized.

2.1. Magnetic reference configuration and input data

The provided magnetic configuration (see Fig. 1) contains the input data for the inverse reconstruction algorithm:

- DTT geometry
- 24 active currents (i_{coil}) from poloidal field coils and central solenoid
- 80 magnetic field measures from 40 pick-up coils (40 measures of the radial component and 40 of the tangential ones)
- mount positions and orientations (with respect to the VV) of the 40 pick-up coils
- mesh nodes domain [4]: n = 29,589.

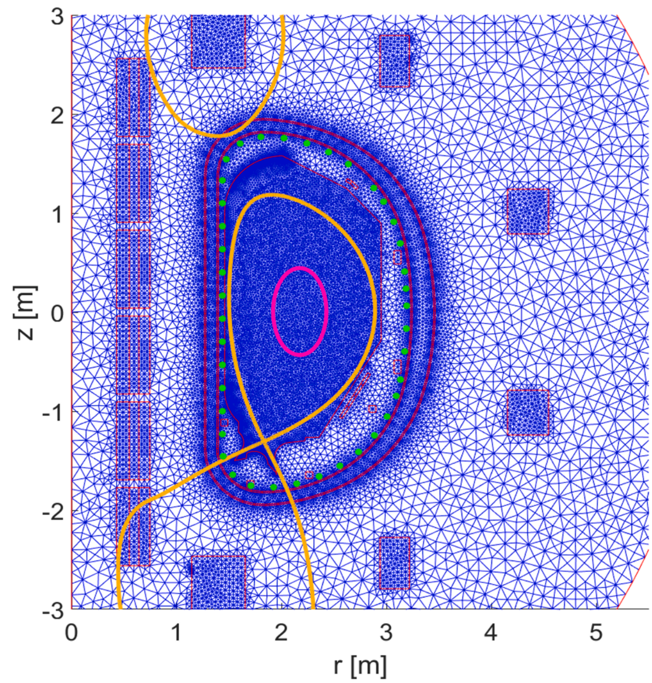

Fig. 1. DTT geometry (red) and the domain mesh (blue). The yellow line is the plasma boundary of the magnetic reference configuration. The green points are the 40 pick-up coils.

2.2. Optimization of pseudo-inverse parameters

The i_{el} currents are evaluated by Eq. (3):

$$|i_{el}|^{n_{el}\times 1} = \left(pinv|G_{0B,el}|\right)^{n_{el}\times n_m} \cdot |B_{plasma}|^{n_m\times 1} \tag{3}$$

where B_{plasma} is obtained subtracting from the poloidal magnetic field (B_{pol}) measurement the contribute due to active current filaments, n_m=*80* is the number of poloidal field measurements $B_{pol,}$ and G_{0B} is a no-square matrix of the Free-Space Green's Functions implemented in [6,7]. The function *pinv* indicates the pseudo inverse operation carried out through the Singolar Value Decomposition (SVD) technique [8]. In the pseudo-inverse operation, a tolerance, which defines the lowest singular value to be considered in the truncated SVD, needed to be defined. In addition to the tolerance value, the performance of pseudo-inversion also depends on the number of fictitious current filaments n_{el}, which must be much lower than n_m. In fact, the higher the number n_{el}, the more the problem is ill-posed, and the larger must be the tolerance to avoid flux map aberration. Thus, a good compromise between the tolerance and n_{el} values needs to be found in order to guarantee a reliable and correct boundary reconstruction. To this purpose, an optimization procedure has been developed that minimizes the difference of the plasma boundary flux values between the inverse and the direct reconstruction. The number n_{el} was varied in the range *10÷30* (with a step resolution equal to 5) and, for each n_{el} value, the size of the singular value vector is optimized in the range *1÷* n_{el} (with a step resolution equal to 1) by changing the tolerance of the pseudo inverse operation.

Fig. 2 shows the errors of the inverse reconstruction with respect to the direct one in terms of difference of the plasma boundary flux values $\Delta\Psi_{bound}$ (upper subplot), distance between X-points ΔX_P (middle subplot) and difference of the plasma currents ΔI_p (bottom subplot), in the n_{el} range *10÷30*. For n_{el} = 30, the magenta vertical line identifies the tolerance that minimizes $\Delta\Psi_{bound}$, instead the green line indicates the tolerance required to avoid flux map aberration. The light blue vertical line corresponds to the tolerance that minimizes $\Delta\Psi_{bound}$ without any flux map aberrations for n_{el} = 10.

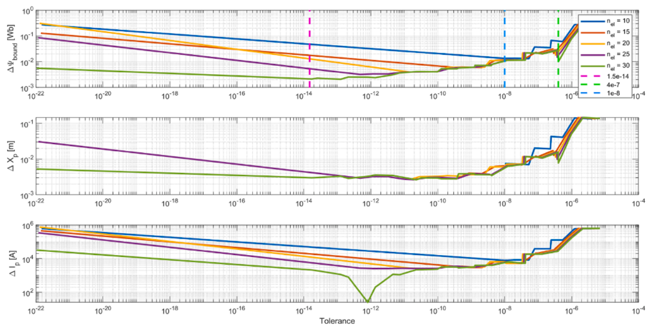

Fig. 2. The trend of the difference of the plasma boundary flux values ($\Delta\Psi_{bound}$, upper subplot), the distance between X-points (ΔX_p, middle subplot) and difference of the plasma currents (ΔI_p, bottom subplot), between the inverse reconstruction and the direct reconstruction, for n_{el} in range 10÷30, at varying tolerance.

Fig. 3 shows, on the left plot, the reconstructed boundary with $n_{el} = 30$ and a tolerance value corresponding to the magenta vertical line in Fig. 2. This unsuitable combination of n_{el} and tolerance values leads to flux map aberration in the plasma center region. In the middle plot of the same Fig. 3, the reconstructed boundary with $n_{el} = 30$ and a tolerance value corresponding to the green line in Fig. 2 is reported. In this case, using a higher tolerance, the flux map aberration is avoided, but $\Delta\Psi_{bound}$ increases, and the reconstructed boundary (green line) does not overlap the reference one (black line). Finally, the right plot reports the boundary reconstruction for the optimum tolerance value (light blue vertical line in Fig. 2) with $n_{el} = 10$. By reducing both n_{el} and the tolerance the numerical error is slightly reduced still avoiding the flux map aberration. The reconstructed boundary (blue line) overlaps the reference one (black line). This reconstructed boundary is used for the white noise characterization of the pick-up coil measurements, described in the following subsection.

2.3. White noise analysis

The presence of white noise on the pick-up coils outputs has been simulated adding a small random contribute to B_{pol}. A parametric study increasing values of probe noise variance (σ^2_{WN}), i.e., 2 mT, 4 mT and 8 mT, has been performed. For each variance value, the inverse reconstruction, optimized as described in Section 2.2, was repeated a thousand times to better simulate the noise random effect on the inverse reconstruction. The noise effect is characterized evaluating the mean error (ME), the mean square error (MSE) and the variance (σ^2_{GAP}) on the gap difference between the noisy optimized inverse reconstruction and the ideal one. These gaps are evaluated on some of the most significative chords, reported in Fig. 4. The ME, MSE and σ^2_{GAP} values, for the different noise variance, are reported in Table 1. Moreover, Table 2 reports, on columns two and three, the maximum and the mean values of the percentage error on the plasma current value, respectively. Whereas the mean errors of the plasma barycenter position (r_0,z_0) are reported in column four and five, respectively.

The results show that errors on the gaps evaluation due to the white noise effect is quite negligible since, for the noise variance values

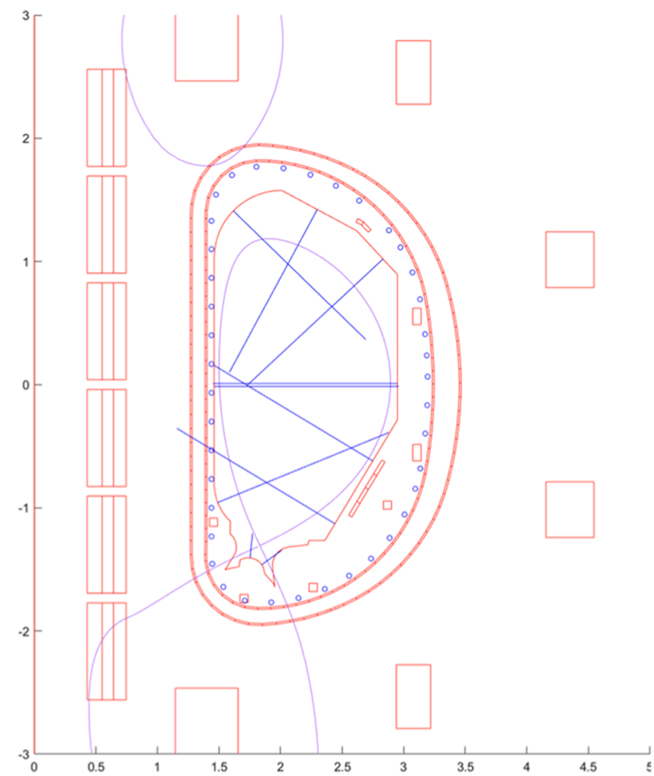

Fig. 4. Chords considered for gaps evaluation.

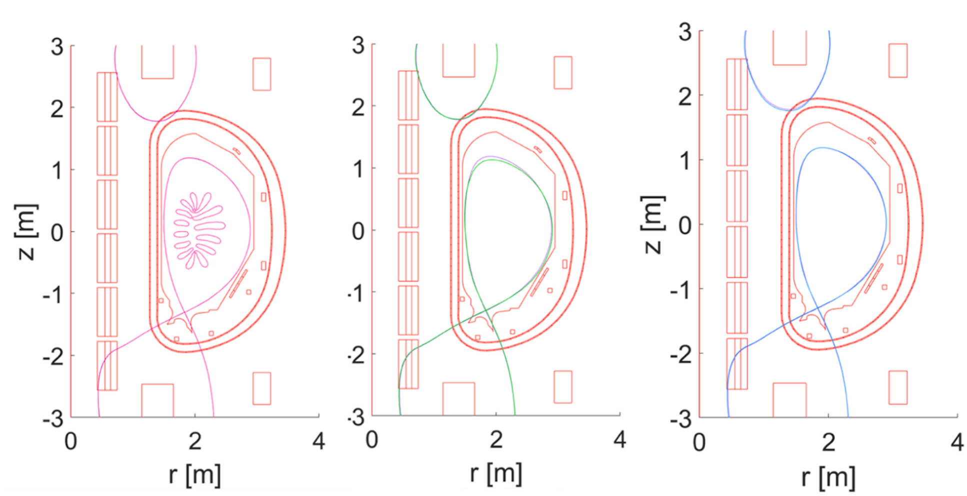

Fig. 3. Inverse boundary reconstruction for different combinations of n_{el} and tolerance values. Left plot: a flux map aberration in the plasma center is obtained with $n_{el} = 30$ and a tolerance value of about 10^{-14} (magenta vertical line in Fig. 2). Middle plot: the flux map aberration is avoided with a tolerance value of about 10^{-6} (green line Fig. 2). Right plot: optimum flux map reconstruction achieved with $n_{el} = 10$ and a tolerance value of about 10^{-8} (light blue vertical line in Fig. 2).

Table 1
Gap errors.

[mT]	ME [mm]	MSE [mm]	σ^2_{GAP} [mm]
2	$-6\ 10^{-1}$	$1.4\ 10^{-2}$	$7.5\ 10^{-4}$
4	-7	$5.8\ 10^{-3}$	$3.0\ 10^{-3}$
8	-7	$2.4\ 10^{-2}$	$1.3\ 10^{-2}$

Table 2
Maximum and mean error on the plasma current value and plasma current barycenter position (r and z coordinates).

[mT]	$\%Ip_{err,max}$	$\%Ip_{err,mean}$	$\delta r_{0,mean}$ [mm]	$\delta z_{0,mean}$ [mm]
2	0.147	0.027	0.4	0.35
4	0.244	0.055	0.8	0.7
8	0.469	0.108	1.6	1.5

considered, the ME, MSE and σ^2 result to be lower than 7 mm. Instead, the$\%Ip_{err,max}$ ($>$ 0.1%) appears to be not negligible for all the considered conditions.

3. Bulk analysis for mounting external pick-up coils

The feasibility of mounting ex-vessel probes in terms of bulk has been investigated. The VV dilatation, determined by FEM analysis, allows us to verify the possibility of assembling the pick-up coil on the vessel between the thermal shield (TS) and external VV wall. The distance of these two components is about 2 cm, and the thermal gradient is about 300 °C. In this analysis, the VV and the ports are modelled as a unique surface body. This assumption leads to some important advantages: no contacts need to be defined between VV and ports; a mapped mesh with aspect ratio approximately equal to one can be easily obtained, which allows a reduction of at least 33,3% of the elements number. Moreover, a 120° VV portion is considered, as the entire vessel can be obtained with an axisymmetric revolution around the toroidal axis.

In addition, considering different temperatures and assuming a welding as mounting solution, the mechanical stresses on the pick-up coil and the screw, due to both the VV dilatation and the different thermal expansion of the VV and the screw, have been preliminarily evaluated.

3.1. Technical assumptions

For the steady-state thermal analysis, three different vessel temperatures are considered: 50 °C as operative temperature, 110° e 220 °C as baking temperatures. The environmental temperature is −200 °C. Since vacuum condition is assumed, no convection is considered, and every thermal exchange is conductive or radiative. Table 3 shows the emissivity assumed for each material defined in the model. The coil will be realized by enameled polished copper, thus a reduced emissivity is assumed for the thermal analysis, to take into account the wire insulation. The pick-up coil is fixed between the shoulder screw and the bolt, and the screw is welded on the VV. To model the welding a bonded constraint has been chosen. To model the welding, a bonded constraint has been chosen.

Fig. 5 shows the mechanical constraints assumed for the VV structure for the static structural analysis: the central sector of the VV portion has a fixed support (blue region), which represents the VV pedestal; each port has a constraint along the edges (yellow line) simulating the flange constraint at the end of the ports. Thus, only displacements along x-axis are allowed as in [9].

Table 3
Emissivity for each defined material.

Torlon (coil support)	Polished copper (coil)	Steel (bolt and VV)
0.5	0.02	0.3

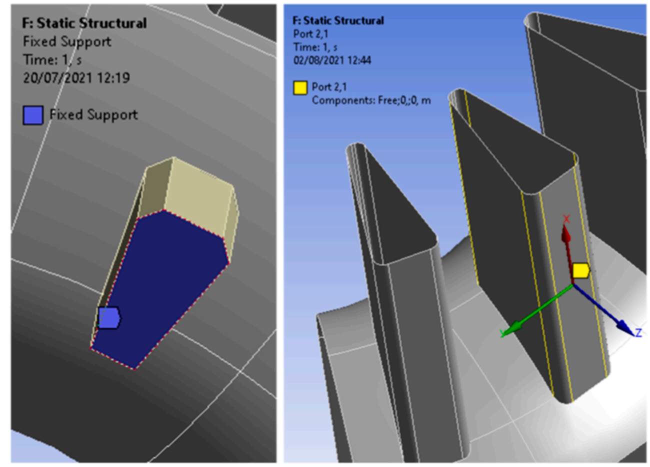

Fig. 5. Left side: VV fixed support (blue region). Right side: port edge constrains (yellow lines).

3.2. Steady-state thermal results

Fig. 6 shows the temperature distribution on the several pick-up coil materials for the backing temperature $T = 220°$: the torlon support in subplot a), the polished copper coils in subplot b), the steel bolt in the subplot c). The temperature distributions on the different materials are qualitatively the same for all the considered operative and backing temperatures, but different minimum and maximum are achieved, as reported in Table 4 and Table 5 respectively. The temperature distribution is imported in static-structural analysis as an external load.

3.3. Results of the static-structural analysis

Fig. 7 reports the VV thermal dilatation; the vectorial representation clearly shows that the displacements are not constant along the profile. The maximum displacements take place just below the equatorial region (where the modelled pick-up coil is located) and in the upper region. Whereas, as expected, in the support region the displacement is the lowest, where the VV is bonded. As found for the pick-up coil temperature distribution, the VV displacement distribution is qualitatively the same for all the considered backing and operating temperatures, but different maximum and minimum displacements are achieved, as reported in Table 6. Note that, no relative displacement is allowed between VV and the pick-up coil, thus a VV displacement causes the same shift of the pick-up coil. The maximum thermal dilatation of the vessel results in 7 mm at the equatorial region for $T = 220$ °C. Since the pick-up coil radial size is 9.6 mm, in the worst condition a free gap of 3.4 mm is still available between the probe and the TS. Thus, no bulk criticality is present for the external pick-up coil mounting. The result of the bulk analysis is not related to the probe mounting solution. The performed thermomechanical analysis allows to determine the stresses due to both the VV dilatation and the mounting solution. Indeed, a complete model of the VV was used instead of the local one, which would have been enough to evaluate the thermal expansion and the thermomechanical stress of the pick-up due to the mounting solution.

The displacement achieved at the operative condition affects the field measurements, thus the displacement and the rotation of the pick-up coil have been evaluated (see Fig. 8), resulting in radial shift of about 1 mm and a rotation of 0.002° A preliminary parametric study has been performed on the error of the inverse boundary reconstruction due to internal pick-up coil rotation, by ranging the pick-up toroidal rotation from one thousandth of a degree to half a degree. This study shows that the error of the inverse boundary reconstruction due to internal pick-up

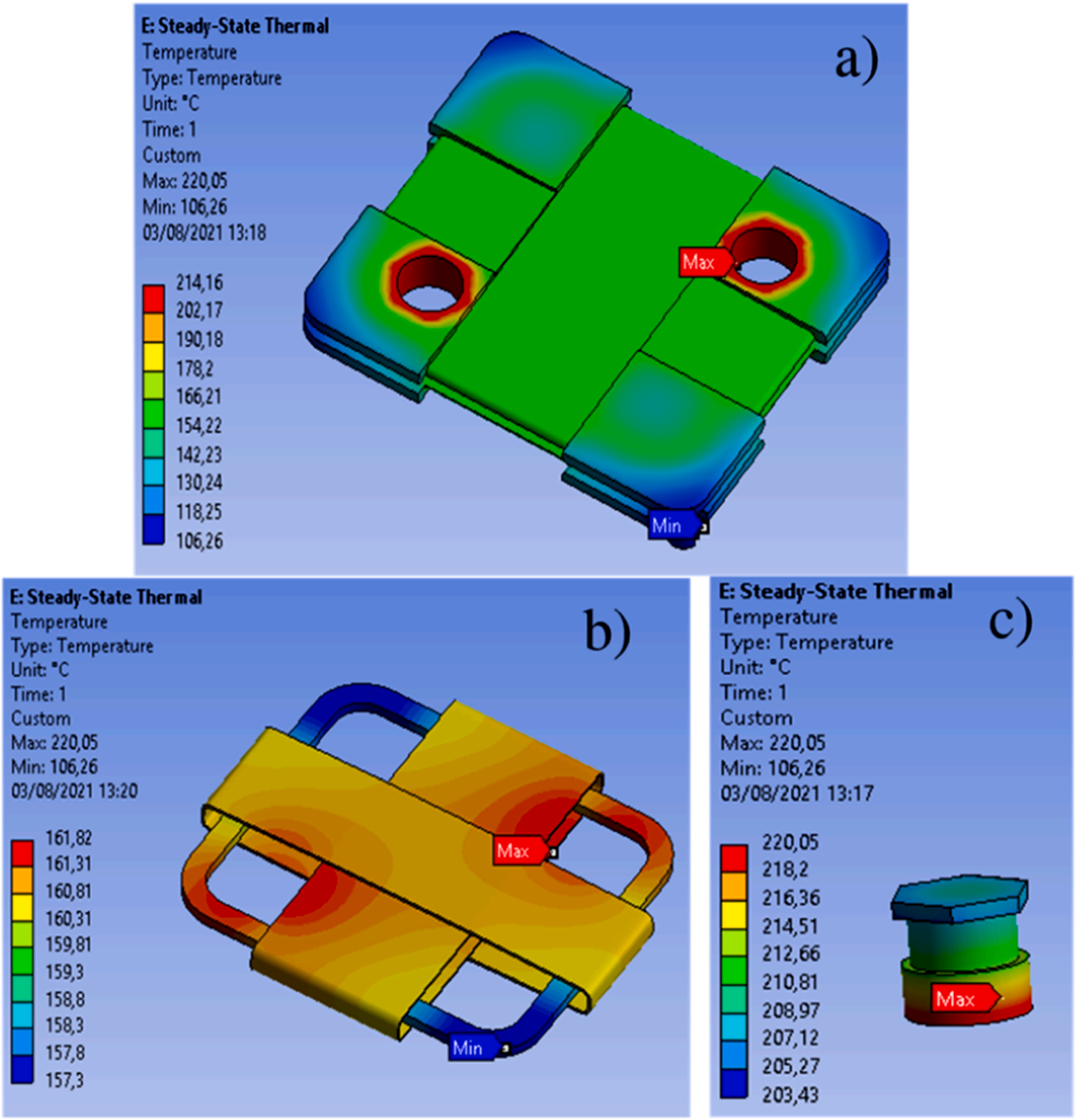

Fig. 6. Temperature distribution on pick-up coils (backing temperature $T = 220$ °C), a) torlon support, b) polished copper coils, and c) steel bolt.

Table 4
Minimum temperature values achieved for each material for operative and backing conditions.

	50 °C	110 °C	220 °C
Torlon	2.6	38.7	106.3
Polished copper	29.7	76.7	157.3
Steel	45.1	101.7	203.4

Table 5
Maximum temperature values achieved for each material for operative and backing conditions.

	50 °C	110 °C	220 °C
Torlon	48.3	107.1	214.2
Polished copper	31.3	79.2	161.8
Steel	50	110	220

coil rotation of few thousandths of a degree can be neglected. This means that the measurement errors due the external pick-up coil rotations of the same magnitude can be neglected. Once the external pick-up coil mounting details will be defined, a dedicated analysis about the inverse boundary reconstruction error due to the external probe rotation and deformation, and the VV displacements will be performed.

Critical stress values on the pick-up coils are achieved only with the backing temperature $T = 220°C$. Fig. 9 shows the equivalent Von-Mises stresses on the bolt. The critical values, $\sigma_{max} > \sigma_{UTS}$ (Ultimate Tensile Strength, 2.6 10^8 Pa [9]), is reached on the screw bottom surface. Note that two different steels were considered for VV (Structural Steel) and for bolt (Stainless Steel). The high stress values are probably also due to

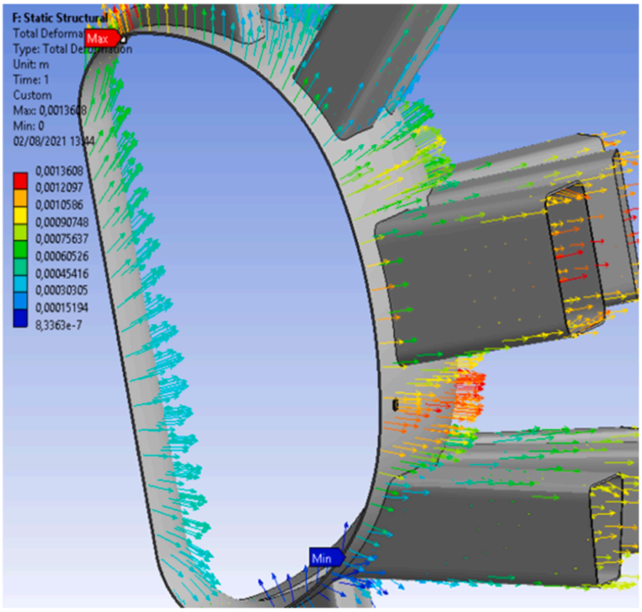

Fig. 7. VV thermal dilatation ($T = 50$ °C).

Table 6
Minimum and maximum displacements (S) occurred on the VV (and pick-up coil) for the backing and the operative conditions.

	50 °C	110 °C	220 °C
S_{min} [mm]	0.1	0.1	0.4
S_{max} [mm]	1.4	4.3	9.6

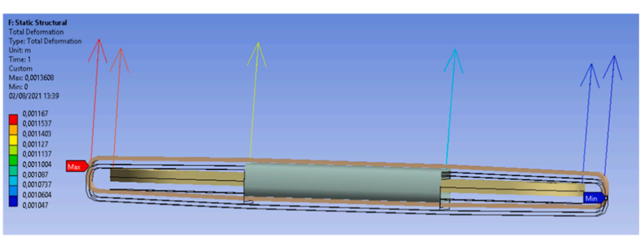

Fig. 8. Static structural results: displacement of ex-vessel pick-up coil ($T = 50$ °C).

the difference between the two steel thermal dilatation coefficients.

Concerning the internal stresses, no criticisms are present in the torlon support, while no statement can be done for the copper coils before defining any further details about the copper wrapping solution.

4. Conclusions

The 2021 DTT reference magnetic configuration consists of 40 internal pick-up coils, resulting in 80 poloidal magnetic field measurements. In this paper, the characterization of the systematic error due to white noise on the optimized inverse boundary reconstruction is presented. The presence of white noise on the pick-up coils output has been simulated adding a small random contribute to the B_{pol} measurements with three different variance values, 2mT, 4mT and 8mT. For each value of the variance the inverse reconstruction was repeated a thousand times to better simulate the noise random effect on the inverse boundary reconstruction. The noise effect has been evaluated in terms of mean error, mean square error and variance on the gap difference between the noisy optimized inverse reconstruction and the ideal one.

The paper reports the thermo-mechanical analysis of external torlon pick-up coils, placed between the TS and external VV wall, for backing and operative conditions assuming a welding as mounting option. The operative temperature ($T = 50$ °C) results in being far from critical condition both in terms of thermal stress and displacement. In fact, the VV and thus the pick-up coils present a radial shift of around 1 mm. This shift leads to a pick-up coil rotation around the toroidal axes of 0.002° At the baking temperature $T = 220$ °C, the gap between the VV and the TS results to be large enough to grant the maximum thermal dilatation of the VV, thus no limit is present for the external pick-up coil in terms of mounting bulk. Instead, criticisms are presents in terms of the bolt stresses due to different thermal expansion of the VV and the screw. A more detailed pick-up coil mounting solution needs to be defined in order to accurately evaluate the stresses on the contact region between pick-up coil and VV. In fact, overcoming σ_{UTS} is critical not only in terms of permanent pick-up coil deformation and displacement, but this can also cause the screw failure. Although the assembly condition of the probe, assumed in this paper, would not be the final one, the thermo-mechanical stresses behavior is a lesson learnt for the next step of the external pick-up coil design.

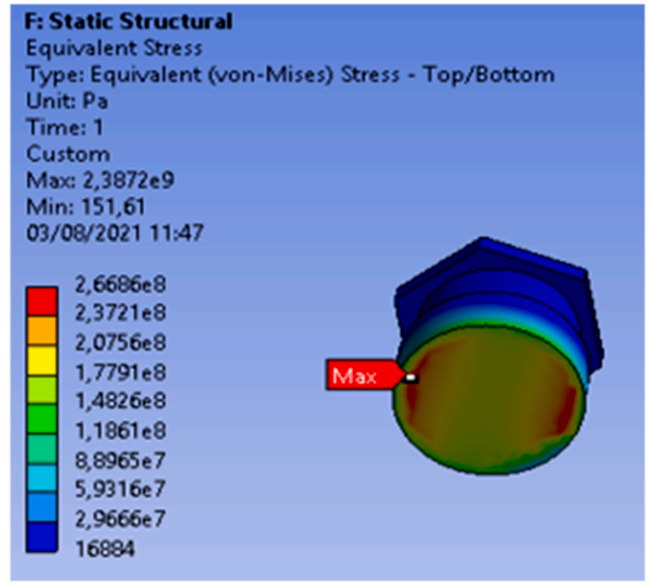

Fig. 9. Equivalent Von-Mises stresses on the bolt for the backing temperature $T = 220$ °C.

Declaration of Competing Interest

The authors declare that they have no known competing financial interests or personal relationships that could have appeared to influence the work reported in this paper.

Data availability

Data will be made available on request.

References

[1] R. Martone, et al., DTT divertor tokamak test facility interim design report, ENEA (ISBN 978-88-8286-378-4). Identification of Filaments from Fast Visual Imaging Cameras in Tokamak Reactors, Esposito A., 2019. In:.
[2] D. Testa, et al., The magnetic diagnostic set for ITER, IEEE Trans. Plasma Sci. 38 (3) (Mar. 2010) 284–294.
[3] A. Mele, et al., Preliminary evaluation of the LIUQE code reconstruction performance for DTT device, Fus. Eng. Des. 167 (2021).
[4] M. Baruzzo et al., Conceptual design of DTT magnetic diagnostics, 46th EPS Conference on Plasma Physics, July 8th- 12th 2019 Milan.

[5] M. Ariola, A. Pironti, Magnetic Control of tokamak. Plasmas, Advances in Industrial Control, Book, Springer-Verlag, 2008.
[6] R. Albanese e, F. Villone, «The linearized CREATE-L plasma response model for the control of current, position and shape in Tokamaks, Nucl. Fus. 38 (1998).
[7] R. Albanese, et al., Plasma response model for current, shape and position control at JET, Fus. Eng. Des. 66 (2003) 725–728.
[8] Steven L. Brunton, J.Nathan Kutz, Data-Driven Science and Engineering: Machine Learning, Dynamical Systems, and Control, Cambridge University Press, 2019.
[9] E. Martelli, et al., Design status of the vacuum vessel of DTT facility, Fus. Eng. Des. 172 (2021), 112760.

Further reading

[1] L. Caligaris, S. Fava, C. Tomasello, Manuale di Meccanica HOEPLI, p. 2021.